RSC Advances

ROYAL SOCIETY OF CHEMISTRY

www.rsc.org/advances

ARTICLE TYPE www. rsc.org/xxxxxx | XXXXXXXX

Cluster dynamics simulation of deuterium retention behaviors in irradiated beryllium

L. Hu[a], Y.G. Li[ab], C.G. Zhang[a] and Z. Zeng[*ab]

Received Xth XXXXXXXXXX 20XX, Accepted Xth XXXXXXXXX 20XX
First published on the web Xth XXXXXXXXXX 200X
DOI: 10.1039/b000000x

The retention behaviors of deuterium (D) in beryllium (Be) are investigated by a spatially resolved cluster dynamics model under different irradiated conditions. The trapping effects of deuterium (D) in the forms of D atoms, D_2 molecules and D with vacancy complex clusters (D_mV) play the most important role on the behaviors of D retention in Be bulk under irradiation of 9-keV D ions. The fraction of D_2 in the total D retention increases with the ascension of ion influence, due to the chemical reaction rate enhancement between D atoms with high density. The increases of both ion incident angle and Be bulk temperature reduce the D_mV complex clusters retention by increasing the D desorption rate. In addition, the neutron synergistic irradiation changes the D retention profiles, especially in the recombination region, by introducing extra defects sinks. These results can improve the understanding of the mechanisms of D diffusion, accumulation and retention in irradiated Be.

1 Introduction

Energy shortage and environmental issues prompt people to spend great efforts on the researches of nuclear fusion energy nowadays. Energetic particles, such as hydrogen isotopes and helium ions, escaped from the fuel during plasma burst events in fusion reactors, would implant into and damage the plasma-facing materials (PFMs)[1,2]. The aggregation of different radiation defects, especially incident ion deposition, can induce strong disruption on the host lattice, thus leading to degradation of PFMs[3]. Beryllium (Be) is considered as one of the promising candidates for PFMs in nuclear fusion reactors, because of its excellent oxygen gettering capability, low sputtering, great mechanical and thermal properties, etc[4]. However the high retention rate of deuterium (D) in Be induces a set of serious problems, such as the formation of surface sputtering, erosion, swelling and blister, etc. To understand D retention behaviors in Be, it is necessary to predict the detailed interactions of D with other defect clusters in Be, quantitatively.

Numerous experimental studies have been done to reveal the accumulation behaviors of radiation damages. For instance, Elastic Recoil Detection (ERD) method has been used to study the D retention behaviors in Be bulk[5], which shew that D can penetrate into the depth of 450 nm and accumulate up to the concentration of $(7-9)\times10^{21}D/cm^3$ under the D flux of $10^{16}Dcm^{-2}s^{-1}$. After that, similar experiments illustrated that deuterium is mainly trapped as D atoms and D_2 molecules in irradiated Be[6]. On the other hand, theoretical studies have also been conducted focusing on the atomic details of D behaviors, such as the solubility, migration paths and correlative kinetic coefficients of D in Be, by using atomic methods such as density functional theory (DFT) and molecular dynamics (MD)[7–11]. However, the long-term behaviors of D in Be and the details of dynamical evolution are yet studied inadequately, which requires to employ a multi-scale model.

In material science, CD model is a mesoscopic model to describe the evolation of defect concentrations by considering the generation, diffudion, reaction and absorption processes of point defects and clusters with a possible event list and corresponding rate coefficients. Compared to the atomic-scale simulation methods, such as density functional theory (DFT) and molecular dynamics (MD) method, CD model is more effective for handling the long-term irradiated damage evolution, which encompasses models from the atomistic to the continuum scale and timescales from diffusion ($\sim ns$) to microstructural evolution ($\sim years$). The high computational efficiency is due to the introducing of the mean field approximation which refers a basic hypothesis of uniform distributions of defects (the real system is replaced by an effective continuously medium), but with the loss of the spatial correlations effect between defects. We can also partly take into account of the spatial correlation effect by partitioning the depth into small intervals in which defect concentration changes through diffusion and reactions. Additionally, the master equations are used to describe the concentration evolution of different point defects and their clusters with time and space. By solving the set of partial differential equations (PDE) constituted by

[a]*Key Laboratory of Materials Physics, Institute of Solid State Physics, Chinese Academy of Sciences, Hefei 230031, China*
[b] *University of Science and Technology of China, Hefei 230026, China*
[*] *Email: zzeng@theory.issp.ac.cn; Tel: +86-551-65591407; Fax: +86-551-65591434*

the master equations numerically, the information about different defect evolution can be obtained and compared with the experimental results straightforwardly. And the method has been successfully applied to simulate long-term evolution of the microstructures of materials [12–17]. Thus, it is much suitable to use this method to study the defects dynamics evolution in irradiated systems.

In this paper, we intend to investigate long-term evolution of D diffusion and retention along depth for Be under different irradiation conditions, by employing CD model. The model is extended from IRadMat program [12,16,18], by taking into account of the corresponding types of defects and by adopting reliable parameters and complex reaction types. Our results highlight the different roles of ion fluence, incdent angle and system temperature as well as neutron synergistic effect to the D retention behaviors in Be.

2 Model and method

We adopt a deterministic cluster dynamics model based on the mean-field rate theory to simulate the retention behaviors of D in Be under energetic particles irradiation [12,13]. A set of partial differential equations (PDEs) constituted by the master equations of different defects in different volume units must be solved numerically. The defect distributions along with depth obtained by the model can be consisted with experimental results, which could provid information about the roles of the different reaction mechanisms. To simplify the calculation, we assumed that the defects of self-interstitial atom (SIA, I), di-interstitials (I_2), vacancy (V), deuterium (D) and di-deuterium (D_2) are mobile, while the complex defect clusters of $I_n (n \leq 100)$, DI and $D_mV (m \leq 5)$ are immobile. Additionally, we only consider defect distribution along with depth for two main reasons. On the one hand, handling a 3D irradiation system by deterministic CD model will increase the computational cost significantly. On the other hand, since Be surface is irradiated under a uniform distribution D ion beam in the experiment, the total D fluence and the induced defects will not change along with the planes parallel to surface. Thus, it is a very reasonable approximation to reduce a 3D model to a 1D model for simplification, as commonly employed elsewhere [13,16]. It is reasonable to neglect the minor intrinsic thermal defects at the beginning of simulation and consider the first-order boundary (correspondence to C(z=0)=0) for simplicity because of relatively high diffusivity of D in Be. Besides, the diffusion coefficients are anisotropy along different specific directions in hexagonal structural system like Be and Zr, which have been studied by Woo et al and Barbu et al. [19–21]. But it is noteworthy that this anisotropic is only considerable for the specific defect especially like SIAs with extreme high diffusivity [20]. In addition, the contribution of SIAs to D retention in Be can be neglected as shown below. Thus, we have ignored the influence of the defect anisotropic diffusivity for the D retention in Be. The basic procedure is demonstrated briefly as follows.

Table 1 Reaction types and the relevant chemical rate coefficients. Reaction coefficients quantify the rate of a chemical reaction for unit concentration, which are mainly dependent on system temperature (T), atomic volume (Ω), cluster binding energy (E_b), defects relative diffusivity (D) and reaction distance (R_{A+B}). In principal, the reactions are described by $A+B \rightleftharpoons AB$ with the forward and backward rate coefficients calculated by $k^+_{A+B} = 4\pi R_{A+B}(D_A + D_B)$ and $k^-_{A-B} = \frac{1}{\Omega} exp(\frac{-E^b_{AB}}{k_B T})$, respectively.

Reaction types	Coefficients Rate
$I+V \rightleftharpoons 0$	$k^+_{I+V}, G_{I/V}$
$I+I_n \rightleftharpoons I_{n+1}$	$\alpha^+_n, \alpha^-_{n+2}$
$I+D \rightleftharpoons DI$	k^+_{D+I}, k^-_{DI}
$V+D \rightleftharpoons DV$	k^+_{D+V}, k^-_{DV}
$I_2+V \rightarrow I$	$k^+_{V+I_2}$
$D+D \rightleftharpoons D_2$	η^+, η^-
$I+D_mV \rightarrow mD$	$k^+_{D_mV+I}$
$I_2+I_n \rightleftharpoons I_{n+2}$	β^+_n, β^-_{n+2}
$V+I_n \rightarrow I_{n-1}$	$k^+_{I_n+V}$
$V+DI \rightarrow D$	k^+_{DI+V}
$D+D_mV \rightleftharpoons D_{m+1}V$	$\gamma^+_m, \gamma^-_{m+1}$
$I+L \rightarrow LI$	L_I
$I_2+L \rightarrow LI_2$	L_{I_2}
$D+L \rightarrow LD$	L_D
$D_2+L \rightarrow LD_2$	L_{D_2}

2.1 Master equation

The master equation describes the evolution of defect concentrations with time in irradiated system, including the generation, diffusion, reaction and absorption of different kinds of defects [12,13,16,17,22], which is given by,

$$\frac{\partial C_\theta}{\partial t} = G_\theta + D_\theta \nabla^2 C_\theta + \sum_{\theta'} [w(\theta', \theta) C_{\theta'} - w(\theta, \theta') C_\theta] - L_\theta \quad (1)$$

where $C_\theta (\theta = I, I_2, V, D, D_2, I_n, DI, D_mV)$ are the concentration of defect θ in the irradiated system at specific depth and time; the G_θ, D_θ, and L_θ represent the production rate, diffusion and inherent absorption coefficients (including dislocations and grain boundary) of the defects θ, respectively. $w(\theta, \theta')$ is the transition rate coefficient per unit concentration of defect cluster θ into the defect cluster θ'. In order to further decrease the computational cost, the Fokker-Plank approximation is adopted in our model to transform these discrete master equation into continuous equations.

Table 2 Correlated parameters used in the case of D ions and neutrons irradiated on Be.

Parameters	Symbol	Value	Refs
D beam intensity	I_D	$10^{18} \sim 10^{20}$ $m^{-2}s^{-1}$	21
Temperature	T	300 K	23
Lattice parameter	a_0	2.27Å	24
	c_0	3.56 Å	
D radius	r_D	0.53 Å	13
Burgers vector	b	1.78 Å	24
Dislocation line density	ρ_D	10^{13} m^{-2}	25
Recombination radius	r_{IV}	4.54 Å	–
Formation energy of SIA	E_I^f	5.24 eV	26
Formation energy of Vacancy	E_V^f	0.81 eV	27
Formation energy of D	E_D^f	1.71 eV	27
Migration energy of SIA	E_I^m	0.02 eV	27
Migration energy of Vacancy	E_V^m	0.8 eV	27
Migration energy of D	E_D^m	0.41 eV	4
Binding energy of D_2	$E_{D_2}^b$	2.3 eV	27
Binding energy of $D-V$	E_{DV}^b	1.27 eV	8
Binding energy of $D-D_2V$	$E_{D-D_2V}^b$	0.93 eV	8
Binding energy of $D-D_3V$	$E_{D-D_3V}^b$	0.77 eV	8
Binding energy of $D-D_4V$	$E_{D-D_4V}^b$	0.54 eV	8
Binding energy of $D-D_5V$	$E_{D-D_5V}^b$	0.42 eV	8

2.2 Rate coefficients

According to the above assumptions, the reaction types and rate coefficients are listed in Tab.1. The rate coefficients describe the occurrence probability of the corresponding reactions. The forward and backward chemical reaction rate-coefficients can be calculated using the theory of diffusion-limited reaction and chemical equilibrium principles, respectively. In addition, the generation rate of point defects during irradiation, $G_{I/V}$, determined by using TRIM code[28].

2.3 Numerical method

The master equations describing the evolution of different defects compose a set of PDEs. To improve the compuational efficiency, the PDEs can be transformed to a set of ordinary differential equations (ODEs) by the Taylor series expansion up to second-order terms[29,30]. In this paper, the set of ODEs are solved by using *lsoda* subroutine packages[31]. The method is efficient enough for handling $\sim 10^3$ ODEs here, with no more than one hour on a modern personal computer.

3 Results and discussions

CD model is a meso-scale method[32], in which most of the input parameters should be suitably chosen from the values of experiments or atomic calculations, and the recommended parameters are listed in Tab. 2. The accuracy of CD model

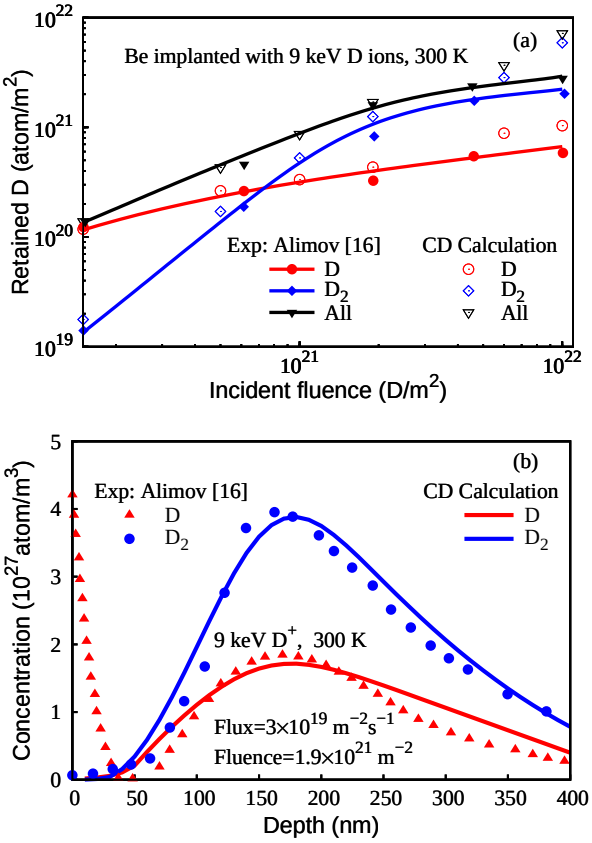

Fig. 1 (a) The total amount of deuterium and fraction quantities of deuterium trapped as D atoms and D_2 molecules. (b) Concentration profiles of deuterium trapped as D atoms and D_2 molecules in a flux of $3\times10^{19}Dm^{-2}s^{-1}$ upto the fluence of $1.9\times10^{21}Dm^{-2}$. D atom implanted into beryllium with the energy of 9 keV at 300 K.

is mainly dependent on the reliability of parameters selected, especially the critical parameters including the defect formation energies and migration energies of mobile point defects (I, I_2, V, D and D_2) which dominate the reaction dynamics processes mostly. By considering the published atomic-scale computational and experimental results, the critical defect types, the reaction event lists and the corresponding reaction coefficients are selected seriously. For example, in order to fit the experiments much well, the D migration energy (E_D^m) are adjusted in the reasonable range of about $0.29 \sim 0.41eV$ and set as $0.41eV$[4,8,27], by considering the presence of impurities and inherent defects probably affects the incident D

diffusion in Be, as pointed out by Orita et al.[33]. In addition, these parameters had been commonly adopted elsewhere[34]. The ab initio results predicted that the maximum number of D surround a vacancy to form a stable cluster is five with the bind energies between 1.27 to 0.42 eV listed in Tab. 2[8]. Besides,the binding energies of mobile point defects (I, I_2) with diffferent types of large loops (I_n) can be obtained by the capillary law approximation[35,36].

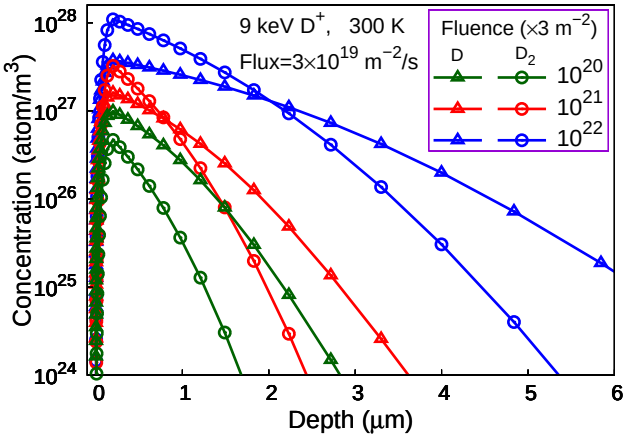

Fig. 2 The depth profiles of atom D and molecules D_2 at different fluence under a flux of $3\times10^{19} Dm^{-2}s^{-1}$ with incident energy of 9 keV at 300 K.

To verify our model, we plot the D retention profile with implanted fluence and the concentration profile of D trapped as D atoms and D_2 molecules in the near-surface region to compare with experiments. It is shown in Fig. 1(a) that the total amount of deuterium retention increases linearly with the increasing of D fluence, which agrees with the experiment well when D beam fluence is low[23,37]. But for high fluence, the experimental relation deviates linear to reach a constant value, due to the surface reconstruction under high flux D ions erosion which prevents the diffusion of implanted D into bulk regions. Furthermore, the saturation of the trapping sites also makes the retention decreasing when a much higher density of D atom accumulated in the near-surface region[13,37].

Fig. 1(b) shows the concentration of deuterium along with depth near-surface. Deuterium prefers in the form of D_2 molecules trapped in the near surface of Be under D ion irradiation in a flux of 3×10^{19} $m^{-2}s^{-1}$ upto the fluence 1.9×10^{21} D m^{-2}. These results are compared well with those of experiment[37], except for a discrepancy near the surface region. It is a common phenomenon for the enhancement of implanted particles at the near surface in irradiation target in the measurements[13]. The difference between the experimental and calculated D concentration at the near surface are mainly coming from the surface roughness, which enhances the adsorption of D atoms on the Be surface in the experiments, and partly from the choice of the free boundary condition on the system surface in the calculation. Furthermore, plasma-surface interaction (PSI) induce the surface configuration reconstructing into a new fluctuated surface, which can hamper the implanted D atoms and make the enhancement of D accumulation at the near surface. Due to materials used for nuclear reactors are generally subjected to be generation of non-equilibrium concentration of atomic defects[?], the concentration ratio between D and D_2 will continually with with differet conditions (ion flux, fluence, incident angle and target temperature, etc.) and with roughly with a special value of 0.5 under the given experimental condition here.

The distribution of the deuterium along the depth in Be irradiated at different D fluence is shown in Fig. 2. With the increasing of D fluence, the D deposition extends into a deeper region. There is a peak at several hundred *nm*, which comes from the self-accumulation and the trapping by other D related defect clusters, that is, D_mV, DI and LD. Consequently, the concentrations decrease with the increasing of depth, which is mainly due to two competitive processes, i.e. the compensation by diffusing from surface and the loss by diffusing away to bulk. For low D fluence of $3\times10^{20}m^{-2}$, D atom concentration is always higher than that of D_2 molecule. Whereas for high D fluence, the concentrations of D and D_2 reverse at a certain depth, because of the relative high ratio of D to D_2 concentration, increasing the conversion rate of $D+D\rightarrow D_2$.

To clarify the contributions of different kinds of D related defect clusters to the D total depth distribution, we plot the detailed depth profiles of D related defect clusters retained in Be in Fig. 3(a), which shows that D atoms, D_2 molecules and the D_mV clusters govern the depth distribution of D in Be. The concentration of deuterium trapped in these three forms is over one order higher than that of trapped by dislocation lines and SIAs.

In nuclear fusion reactors, the synergistic neutron irradiation will further aggravate damages and hydrogen isotopes retention in Be. Its kinetic energy is so high (14.1 MeV) that the neutron in the fusion reactions can easily pass through the PFMs. Consequently, the defects induced by the neutron can be considered as uniform everywhere in a constant rate ($G_{neutron}$), which is usually described by the unit of dpa (displacement per atom). We set neutron irradiation as increasing from a non-zero rate in the non-neutron case to generate defects. Thus, we have also considered this synergistic effect of D and neutron irradiation in the model. The evolution and depth-distribution of defects have been obviously changed under the synerigistic neutron irradiation as shown in Fig 3(b). The extra point defects induced by neutron can further trap D atoms, and can compensate the valley (in the range of several microns) of D_mV clusters formed by the recombination of SIAs and vacancies as shown in Fig. 3(a). While, the influ-

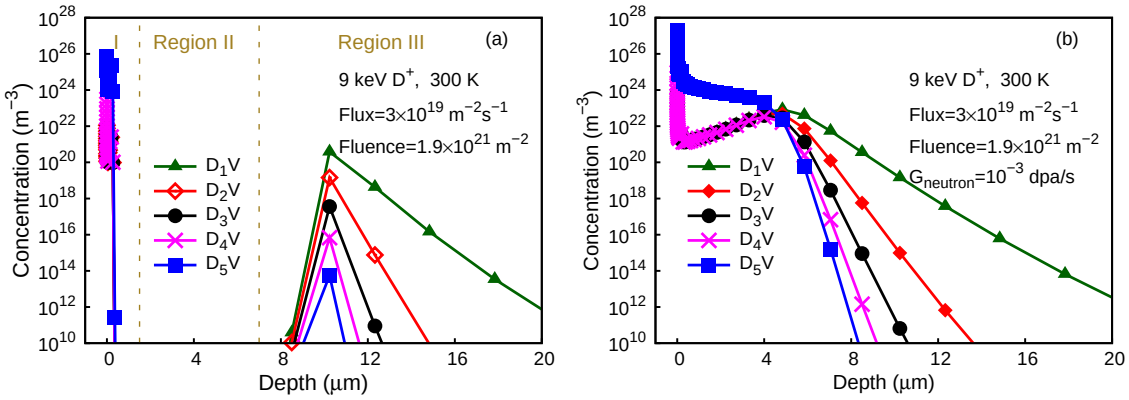

Fig. 4 The depth profiles of deuterium-vacancy complexes D_mV under a flux of $3\times10^{19}Dm^{-2}s^{-1}$ upto the fluence of $1.9\times10^{21}\ Dm^{-2}$ with incident energy of 9 keV at 300 K. (a) without and (b) with synergistic neutron irradiation in the damage rate of $10^{-3}\ dpa/s$.

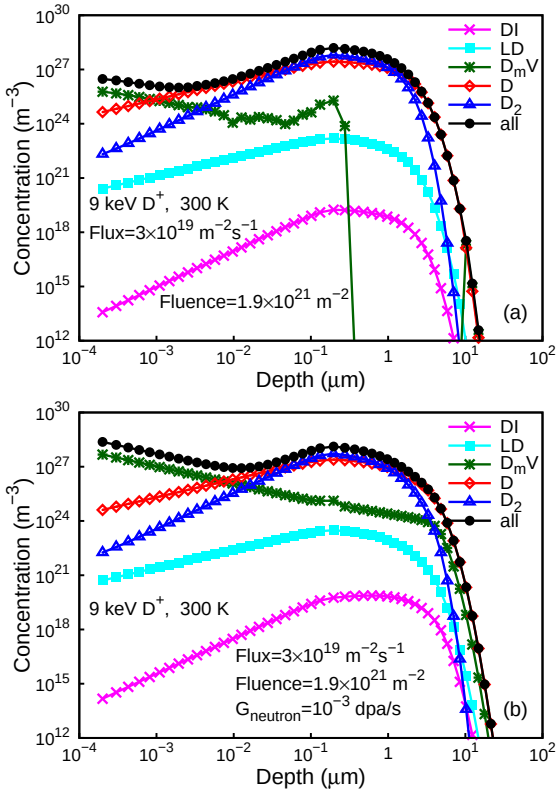

Fig. 3 Details of the depth profiles of D retained in Be under a flux of $3\times10^{19}Dm^{-2}s^{-1}$ up to the fluence of $1.9\times10^{21}Dm^{-2}$ with incident energy of 9 keV at 300 K, (a) without and (b) with synergistic neutron irradiation in the damage rate of $10^{-3}dpa/s$.

ence of synergistic neutron irradiation is feeble for the depth-distribution profiles of the other D related defect clusters, due to the weak sink strengh. Therefore, the synergetic effect of neutron irradiation can change the D distribution forms considerably but the amount of D retention slightly.

Fig. 4(a) illustrates that the distribution of D_mV along with depth can be tentatively divided into three regions according to their respect features (see the dashed line divided areas), i.e. (1) a peak in the surface layer (Region I), (2) a valley in several microns (Region II), which can be called recombination region and (3) a decay along depth entering the bulk (Region III)[13,38]. In Region I, D_5V dominates the concentration of D retained in Be, because of the super-saturation of D in this region during high flux D implantations. In contrast, D_mV clusters prefer to form smaller-size clusters in Range III because of the relatively lower ratio of the concentration of D to V. While Range II, almost all of the vacancies are combined by numerous SIAs migrating rapidly from the surface layer, which causes the formation of sink valley[38]. On the contrary, the extra vacancies introduced by synergistic neutron irradiation can compensate the sink valley, increasing the D retention in this region as shown in the Fig. 4(b).

On the other hand, Be usually serves under the conditions of D plasma with random incident angles and different localized temperatures under high-heat loads in the nuclear fusion reactors. Since the 1D semi-infinite diffusion-reaction system with free boundary condition was considered, the D atoms diffuse towards surface and depart from the bulk directly. In the following, we will consider these two factors for the illustration of their influence on the retention behaviors of D in irradiated Be.

The initial depth-distribution of D retentions in Be with different incident angles, calculated by TRIM code[28], is shown in Fig. 5(a). With the incident angles increasing, the incident D prefers to accumulate near surface and the total D

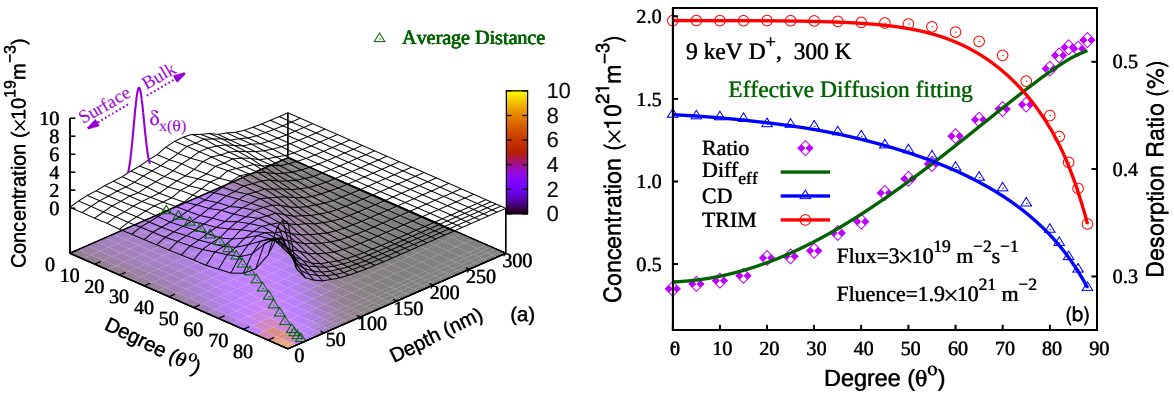

Fig. 5 Concentration profiles of deuterium retention in Be implanted under a flux of $3\times10^{19}Dm^{-2}s^{-1}$ upto the fluence of $1.9\times10^{21}Dm^{-2}$ with the energy of 9 keV at 300 K along with the different incident angles, (a) initial depth-distribution of D and (b) considering the long-term dynamical evolution.

retention decreases gradually due to the back-scattering effect. The diffusion and reaction effects taken account in our CD model aggravate the reduction of D retention in Be, by further absorbing D near surface from Be, as shown in the Fig. 5(b). The relation of D retention in Be with different incident angles can be fitted by an effective diffusion model as,

$$P_t(\theta) = (1-\alpha)\frac{0.35+0.000154\overline{r_\theta}}{0.386} + \alpha\int_0^{\overline{r_\theta}}\frac{exp(-r_\theta^2/4D_{eff}t)}{(\pi D_{eff}t)^{1/2}}dr_\theta \quad (2)$$

where $P_t(\theta)$ represents the retention ratio of D in irradiated Be after time t, α is the ratio of D atom diffusion into bulk (about 0.51), $\overline{r_\theta}$ is average depth of implanted particles which related to the incident angles, and D_{eff} represents the effective diffusion coefficient, fitted by the value of $\sim 9.07\times10^{-14}m^2s^{-1}$. It is reasonable for the effective diffusion coefficient smaller than the value of $1.92\times10^{-13}m^2s^{-1}$, after including the absorption by different sinks. As shown in Fig. 5(a), the first term of Eq. (2) represents the fraction of D diffusing into bulk, which follows a linear relation fitted to the inital distribution. The second term is the fraction diffusing to surface as described by the one-dimension diffusion theory. From the results, it can be deduced that considering the factor of incident angles, the contribution of back-scattering effect is greater than that of the long-term diffusion-reaction effect for the D retention in irradiated Be. Additionally, the diffusion-reaction effect can be described by an effective diffusion model, in which the effective diffusion coefficient can be extracted from retention-angle relations. These results should be much helpful for understanding the diffusion and reaction mechanisms during D desorption form Be bulk.

Concerning temperature, the thermal desorption mechanism of D from Be can also be revealed from our results. As shown in Fig. 6, the relative concentrations of D atom to D_2 molecule are reversal, but the total amount of D retention is almost invariable with the increasing of temperature until about 400 K, which is in accordance to the experimental fact of that the distinct D desorption begins at this temperature (see the insert of Fig. 6)[2]. It can be deduced that the temperature below 400 K is not enough to induce thermal desorption, but improving the reaction rate of D atoms to the D_2 molecules. With the temperature higher than 400 K, the amounts of D and D_2 decreases dramatically, due to high diffusing ability of D and D_2 at higher temperature. Besides, the difference of diffusivity for D atoms ($1.92\times10^{-13}m^2s^{-1}$) and D_2 molecules ($1.02\times10^{-14}m^2s^{-1}$) leads to the presence of two thermal desorption peaks at 440 K and 460 K. In addition, it is also found that nearly no desorption occurs for immobile D complex clusters below 500 K, due to their high binding energies.

4 Conclusions

This work has presented the diverse retention behaviors of deuterium in Be under several irradiated conditions, by analyzing the competition of diffusion and accumulation. In the high energy incidence case, the forms of D atoms, D_2 molecules and D_mV mainly dominate the D depth-distribution in irradiated Be becasue of the relatively weak sink strength. The implanted fluence could manipulate the relative proportion of deuterium retention forms between atoms and molecules. Through the surface desorption, declining incidence and temperature variation also have respected to the behaviors of D retention in radiated Be and the trapped forms. Additionally, the synergistic neutron irradiation induces an uniform distribution of extra point defects which compensates

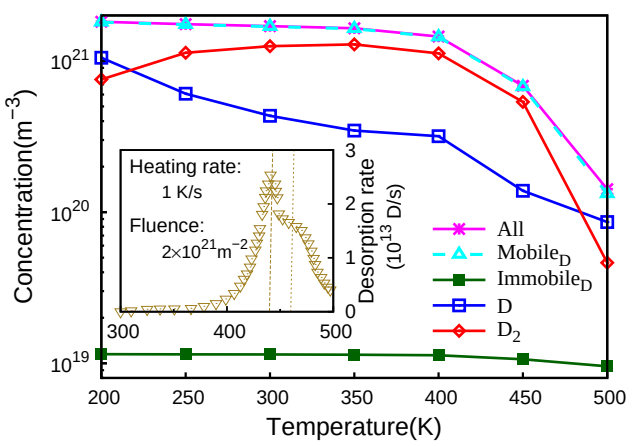

Fig. 6 Detailed temperature profiles of all D, $mobile_D$ defects (D atoms and D_2 molecules), and $Immobile_D$ defects in Be under a flux of $3\times10^{19}Dm^{-2}s^{-1}$ upto the fluence $1.9\times10^{21}Dm^{-2}$ with incident energy of 9 keV. Insert is the experimental desorption rate with a heating rate of $1K/s$ under an incident D fluence of $2\times10^{21}m^{-2\,2}$.

the recombination zone, but affects the deuterium retention slightly. These results will be helpful to understand the long-term dynamic evloution mechanics of defects in PFMs.

5 Acknowledgements

This work was supported by the National Science Foundation of China under Grant Nos. 11275229, 11475215 & NSAF U1230202, the Special Funds for Major State Basic Research Project of China (973) under Grant No. 2012CB933702, and Director Grants of CASHIPS. Part of the calculations were performed at the Center for Computational Science of CASHIPS, the ScGrid of Supercomputing Center, and the Computer Network Information Center of the Chinese Academy of Sciences.

References

1 D. M. Duffy, *Materials Today*, 2009, **12**, 38–44.
2 M. Reinelt, A. Allouche, M. Oberkofler, C. Linsmeier and et al., *New. J. Phys.*, 2009, **11**, 043023.
3 D. M. Duffy, *Phil. Trans. R. Soc. A*, 2010, **368**, 3315–3328.
4 P. B. Zhang, J. Jun, Z. B. Wen and et al., *J. Nucl. Mater.*, 2012, **423**, 164–169.
5 V. M. Sharapov, L. E. Gavrilov, V. S. Kulikauskas and et al., *J. Nucl. Mater.*, 1996, **233-237**, 870–873.
6 V. M. Sharapov, L. E. Gavrilov and V. K. Alimov, *Plasma. Dev. Oper.*, 1998, **6**, 89–94.
7 H. Krimme and M. Fahnle, *J. Nucl. Mater.*, 1998, **255**, 72–74.
8 M. G. Ganchenkova, V. A. Borodin, R. M. Nieminen and et al., *Phys. Rev. B*, 2009, **79**, 134101.
9 M. G. Ganchenkova and V. A. Borodin, *Phys. Rev. B*, 2007, **75**, 054108.
10 P. B. Zhang, J. J. Zhao and B. Wen, *J. Phys. Condens. Matter*, 2012, **24**, 095004.
11 R. A. Anderl, R. A. Causey, J. W. Davis and et al., *J. Nucl. Mater.*, 1999, **273**, 1–26.
12 Y. G. Li, W. H. Zhou, L. F. Huang, Z. Zeng and et al., *J. Nucl. Mater.*, 2012, **431**, 26–32.
13 R. H. Ning, Y. G. Li, W. H. Zhou, Z. Zeng and et al., *J. Nucl. Mater.*, 2012, **430**, 20–26.
14 T. Faney and B. D. Wirth, *Modelling Simul. Mater. Sci. Eng.*, 2014, **22**, 065010.
15 Y. Watanabe, H. Iwakiri, N. Yoshida and et al., *Nucl. Instr. and Meth. in Phys. Res. B*, 2007, **255**, 32–36.
16 Y. G. Li, W. H. Zhou, L. F. Huang and et al., *Plasma Sci. Technol.*, 2012, **14(7)**, 624.
17 R. H. Ning, Y. G. Li, W. H. Zhou, Z. Zeng and et al., *Int. J. Mod. Phys. C*, 2012, **23**, 1250042.
18 Y. G. Li, W. H. Zhou, R. H. Ning and et al., *Commun. Comput. Phys.*, 2012, **11**, 1547–1568.
19 C. H. Woo, *Phil. Mag. A*, 1991, **63**, 915–923.
20 F. Christien and A. Barbu, *J. Nucl. Mater.*, 2005, **346**, 272–281.
21 F. Christien and A. Barbu, *J. Nucl. Mater.*, 2009, **393**, 153–161.
22 T. Faney, S. I. Krasheninnikov and et al., *Nucl. Fusion*, 2015, **55**, 013014.
23 V. N. Chernikov, V. K. Alimov, A. V. Markin and et al., *J. Nucl. Mater.*, 1996, **233-237**, 860–864.
24 R. C. Rau, *Philos. Mag.*, 1967, **16**, 663–667.
25 C. May and P. Klimanek, *Il Nuovo Cimento D*, 1997, **19**, 591–598.
26 S. C. Middleburgh and R. W. Grimes, *Acta Mater.*, 2011, **59**, 7095–7103.
27 M. G. Ganchenkova, P. V. Vladimirov and V. A. Borodin, *J. Nucl. Mater.*, 2009, **386-388**, 79–81.
28 J. P. Biersack and L. G. Haggmark, *Nucl. Instrum. Methods*, 1980, **174**, 257.
29 N. M. Ghoniem and S. Sharafat, *J. Nucl. Mater.*, 1980, **92**, 121–135.
30 M. P. Surh, J. B. Sturgeon and W. G. Wolfer, *J. Nucl. Mater.*, 2004, **325**, 44–52.
31 L. Petzold, *SIAM J. Sci. Stat. Comput.*, 1983, **4**, 136.
32 B. D. Wirth, G. R. Odette, J. Marian and et al., *J. Nucl. Mater.*, 2004, **329-333**, 103–111.
33 C. J. Ortiz, M. J. Caturla, C. C. Fu and et al., *Phys. Rev. B.*, 2007, **75**, 100102.
34
35 C. C. Fu, J. D. Torre, F. Willaime and et al., *Nat. Mater*, 2005, **4**, 68.
36 A. H. Duparc, C. Moingeon and et al., *J. Nucl. Mater.*, 2002, **302**, 143–155.
37 V. K. Alimov, V. N. Chernikov and A. P. Zakharov, *J. Nucl. Mater.*, 1997, **241-243**, 1047–1052.
38 A. Hu and A. Hassanein, *J. Nucl. Mater.*, 2014, **446**, 56–62.